X-ray Telescope Mirror Mounting and Deformation Reduction Using ThermoYield Actuators and Mirror Geometry Changes

Michael D. DeTienne[a,b], Alexander R. Bruccoleri[a], Anjelica Molnar-Fenton[a], Brandon Chalifoux[b], Ralf K. Heilmann[b], Youwei Yao[b], Mark L. Schattenburg[b]
[a]Izentis LLC, PO Box 397002, Cambridge, MA, USA 02139-7002
[b]Space Nanotechnology Lab, MIT, 70 Vassar St., Cambridge, MA, USA 02139

ABSTRACT

Recently, the X-ray optics community has been developing technology for high angular resolution, large collecting area X-ray telescopes such as the Lynx mission concept. To meet the high collecting area requirements of such telescope concepts, research is being conducted on thin, segmented optics. The precision mounting posts that fixture and align segmented optics must be the correct length to sub-micron accuracy to satisfy the angular resolution goals of such a concept. Mirror distortion caused by adhesive shrinkage at mount points on the mirror surface also needs to be controlled to micron-radian tolerances. We report on two solutions to these problems. Set-and-forget adjustable length optical mounting posts have been developed to control mirror spacer length. The actuator consists of a metal cylinder with a cylindrical neck cut halfway along the length. To change the length of this actuator, an axial force is applied and the neck is momentarily heated to the plastic deformation temperature via resistive heating. All of the plastic deformation that occurs becomes permanent after cooling. Both compression and expansion of these actuators has been demonstrated in steps ranging from 6 nm to several microns. This paper will describe an experimental setup, show, and discuss data. Additionally, a stress relief technique to reduce mirror distortion caused by shrinkage of the adhesive bond to the actuator is proposed and demonstrated by modelling.

Keywords: Adjustable, set-and-forget, X-ray telescope, segmented optics, X-ray mirror, optical mount, stress localization

1. INTRODUCTION

1.1 ThermoYield overview

This paper describes the operating principle of ThermoYield actuators which are nano-adjustable set-and-forget optical mounts[1] The concept is to make a cylinder out of metal, and apply a constant axial force in either compression or tension. Next, the metal cylinder is momentarily heated via resistive heating from a pulse of electrical current, which temporarily softens the metal. While soft, the metal plastically deforms and re-hardens when it cools. Repeated adjustments can be made by applying additional electrical pulses. Once suitable adjustments have been made, the constant force can be removed.

ThermoYield actuators are shaped like dumbbells. The larger ends allow for greater attachment area and easier electrical contact. The small neck increases stress and localizes resistive heating. A diagram of this process is shown in Figure 1. In the past, Bruccoleri et al. had used a powerful laser to heat a layer of solder in a process called liquid metal actuation[2]. Electrical heating in ThermoYield actuation has the benefits of heating the entire volume of the material instead of just the surface, delivering the heat further away from the mirrors, working with opaque materials, and being safer for operators.

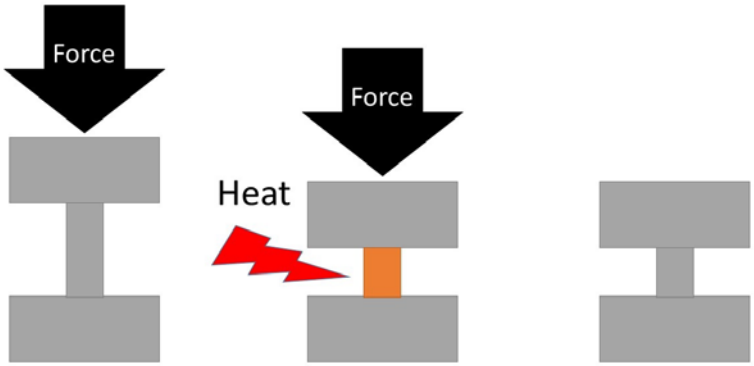

Figure 1. Conceptual drawing of ThermoYield actuation. First, a constant axial force is applied to the actuator, causing a stress in the neck of the sample. Next, the neck is quickly heated, which temporarily reduces its strength. The applied force then plastically deforms the neck. When the neck cools, it regains strength and stops deforming. The sample is now permanently shorter.

The target application of ThermoYield actuators is the precision alignment and mounting of thin-shell X-ray telescope mirrors. The idea of using thin, segmented optics for X-ray telescope construction has already been demonstrated by the NuSTAR X-ray telescope[3]. The NuSTAR X-ray telescope was constructed by stacking thin slumped-glass mirrors on top of each other in layers, using graphite spacers between each layer. NuSTAR achieved a large effective area using this technique[4], however its angular resolution was low, approximately 50 arcseconds HPD[5]. At present, the X-ray astronomy optics community is working towards the Lynx X-ray telescope mission concept with greater than two square meter effective collecting area and angular resolution of 0.5 arcseconds HPD[6].

In order to meet these ambitious collecting area and angular resolution requirements, several different approaches are being developed to build X-ray telescope optics. One particularly promising approach is the meta-shell approach described in detail by McClelland et al.[7] In the meta-shell concept, a radially symmetric mandrel is mounted on a precision spindle. This allows the mandrel to rotate about the optical axis. Then, four small posts are epoxied to the mandrel. Next, the posts are precision machined to the correct height and a thin monocrystalline silicon mirror is epoxied to the top of the posts. The mandrel is rotated and this process is repeated until mirrors are attached around the entire perimeter of the mandrel. After the first layer is complete, a second layer is added on top of the first layer using the same procedure. This stacking is repeated until tens of layers are constructed. Finally, several of these meta-shell assemblies will be concentrically nested and aligned to produce a large X-ray telescope focusing optic.

ThermoYield actuators are designed to serve as the four posts supporting each silicon mirror segment. The height of meta-shell mirror mounting posts must be controlled to sub-micron accuracy[8]. ThermoYield actuators have demonstrated the necessary adjustability, down to 6 nm steps. Additionally, ThermoYield actuators could adjust mirror alignment after initial assembly. This allows a mirror to be adjusted under real-time metrology, even after bonding.

Another potential application of ThermoYield actuators would be the precision aligning of larger optical assemblies. For example, the ATHENA X-ray telescope will consist of 1062 individual mirror modules that must be co-aligned to within 1.5 arcseconds[9]. Current integration methods using epoxy do not allow for adjustments after the mirror modules are epoxied in place. By using ThermoYield actuators, these mirror modules could be adjusted even after the modules are installed.

1.2 Stress localization mirror geometry overview

To address mirror distortion due to bonding, a new idea for stress localization in thin X-ray optics is presented. When epoxy is used to mount X-ray optics to posts, the epoxy introduces a compressive stress on the surface of the optics. From the epoxy stress a tensile reaction on the backside creates bending and distortion. This stress degrades telescope resolution by causing deformation over the entire mirror surface. Two mirror geometry changes are proposed to reduce distortion from bonding stress. One proposal is to cut small circular moats on the front and backside of the optic. These moats will surround the epoxy bond area, and partially localize the deformation to the area encircled by the moat. The second proposal is to cut two parallel slits all the way through the mirror. This will form a bridge on which the mirror is bonded. This geometry will partially localize the deformation of the mirror to the bridge.

2. EXPERIMENTAL SETUP

2.1 ThermoYield experimental apparatus construction

An experimental apparatus was built to demonstrate and evaluate the ThermoYield actuator concept. The apparatus measured the length changes of a ThermoYield actuator with a noise floor of approximately 2 nm. It also recorded the force applied to the actuator, and the amount of energy stored in a capacitor for the electrical heating pulse. The apparatus constrains the actuator to move axially by fixing one end and attaching the other end to a freely-moving linear stage. To measure length changes of the actuator, a capacitive displacement sensor was rigidly mounted to the moving end of the sample, and measured against a micrometer rigidly attached to the fixed end of the sample. The micrometer was used to adjust the capacitive displacement sensor air gap, not to measure the length change of the sample. The micrometer was pre-loaded with a spring in order to reduce backlash. A constant compressive or tensile force was applied to the sample using springs, and measured using a load cell. Finally, a high-current electrical system was connected to each side of the sample. This apparatus is shown in Figure 2.

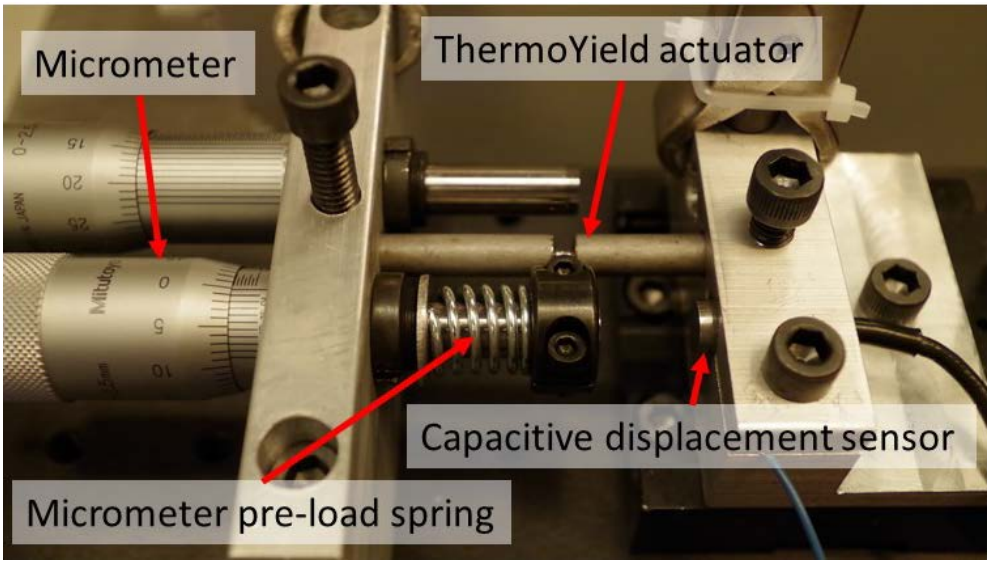

Figure 2. Photograph of the ThermoYield testing apparatus. The micrometer has been pre-loaded using a spring. The capacitive displacement sensor measures the distance to the micrometer face. The gap between the capacitive displacement sensor and the micrometer is exaggerated in this diagram, and is on the order of tens of microns during experiments.

2.2 ThermoYield experimental apparatus electronics

A 0.2 F, 200 V max capacitor bank was built using 10 large electrolytic capacitors in parallel. A SCR with a 46,000 A pulse current rating was used to initiate the electrical pulse. The SCR was triggered by a 9 V battery on a momentary switch, passed through an isolated pulse transformer. The system was built into a metal case, and charged using a 160 V, 5 A adjustable bench supply. The capacitor bank can be charged to any voltage between 0 V and 160 V, allowing significant flexibility in how much energy could be delivered to the sample. A photograph of the electrical system is shown in Figure 3.

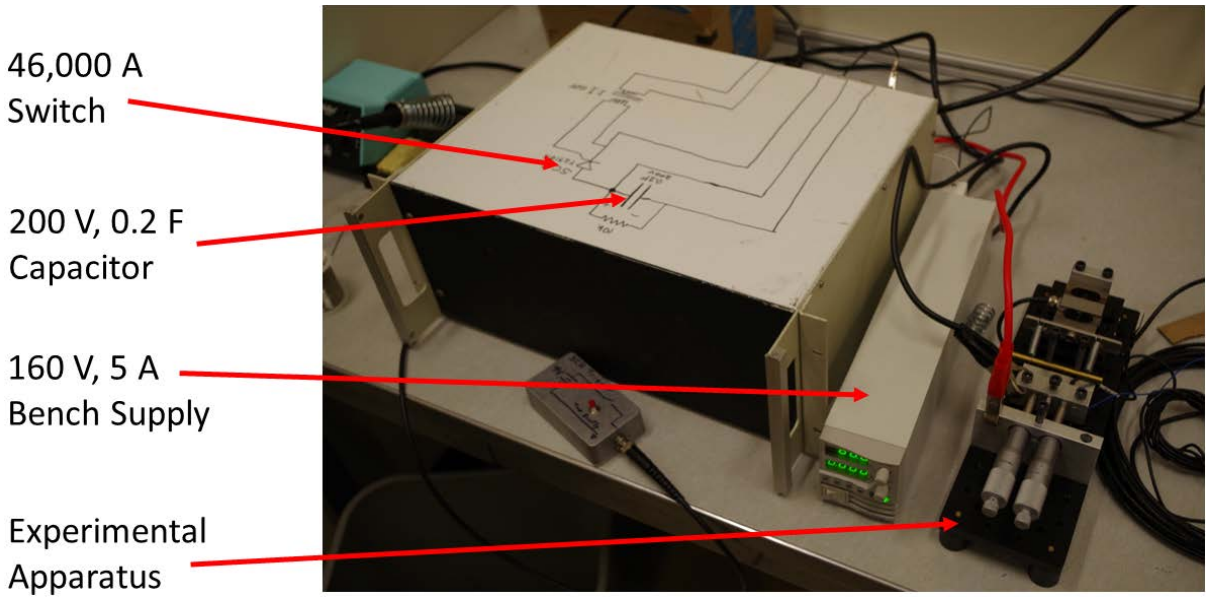

Figure 3. Photograph of ThermoYield electrical system. The capacitor bank and switch used to deliver current pulses are housed inside of a metal box.

2.3 ThermoYield experimental samples

A ThermoYield actuator was machined out of FN381, an iron-nickel alloy with a coefficient of thermal expansion (CTE) similar to silicon to avoid mirror distortion. The actuator is 6.4 mm in diameter and approximately 52 mm long with a neck of 0.9 mm in diameter and 1.1 mm in length.

Additional ThermoYield actuators were constructed out of tungsten and aluminum. The tungsten actuator was made from a pure, polycrystalline 6.4 mm diameter rod. A neck of diameter 1.1 mm and length 1.2 mm was ground into the rod. The aluminum actuator was made from a 6.4 mm diameter rod of 6061-T6 aluminum. The neck was saw-cut to 1.0 mm in diameter and 0.8 mm in length.

3. EXPERIMENTAL PROCEDURE AND DATA

3.1 ThermoYield experimental procedure

The FN381 ThermoYield actuator was loaded into the experimental apparatus and left in a ±1 °C cleanroom overnight to reach thermal equilibrium. During the experiment, the apparatus was covered with a plastic enclosure to further prevent temperature changes. The force applied to the ThermoYield actuator was determined by slowly increasing the force on the actuator until it started creeping more than 5 nm every 100 s, then backing off until the rate of creep was lower than the 2 nm noise floor. For the FN381 actuator, this procedure resulted in a compressive stress of 42.6 MPa in the actuator neck. The capacitor bank voltage was repeatedly increased and discharged through the actuator causing actuations from immeasurably small to over 50 nm. Several actuations were recorded in the same experiment, at the same applied force and varying capacitor bank voltages. Figure 4 shows data for the FN381 actuator (described in section 2.3) under compressive load. Each blue dot represents the change in length of the sample caused by one capacitor bank discharge. Each orange square represents the amount of energy stored in the capacitor bank immediately before discharging. The force applied to the sample was constant during this experiment. All actuations were preformed in succession without touching the apparatus, with approximately 100 s between each actuation

Most of the energy from the capacitor bank is dissipated in the wires and does not contribute to actuator heating. The energies plotted should be viewed as relative values.

3.2 ThermoYield experimental data

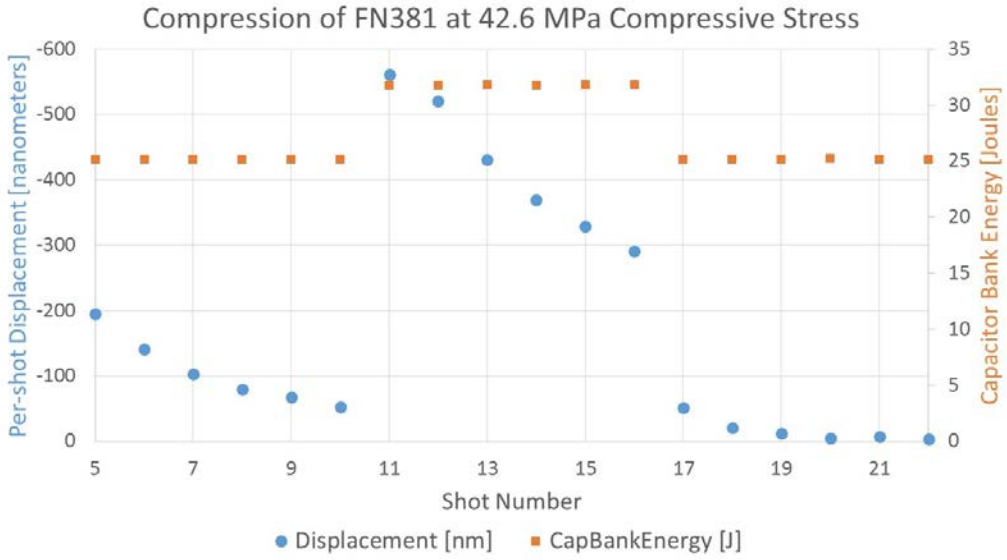

Figure 4. Data[1] gathered using the experimental procedure described in Section 3.

After the experiment from Figure 4, a zero force experiment was performed by removing the compression spring from the apparatus. The capacitor bank was charged to the same energy that was used in the end of the previous experiment and discharged through the unloaded actuator. This unloaded-actuator discharge was repeated several times. The data from this procedure is shown in Figure 5.

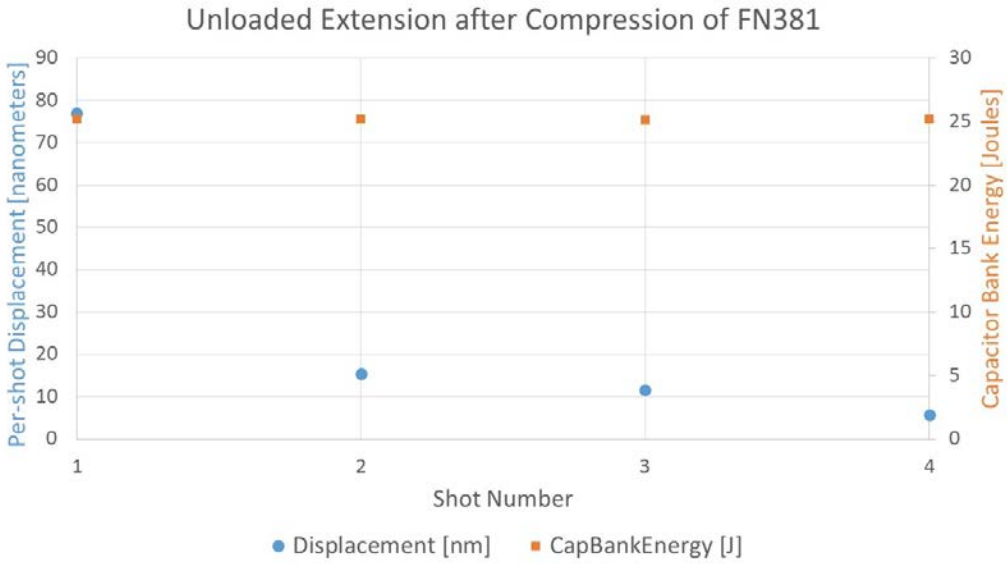

Figure 5. Data[1] gathered with no applied force on the sample. This experiment was performed immediately after the compressive actuations in Figure 4. These no-force actuations moved in the opposite direction of the ones in Figure 4.

The sample was then put under tensile load following the same procedure, including doing much smaller capacitor bank voltage increases and decreases. The data for those actuations is shown in Figure 6.

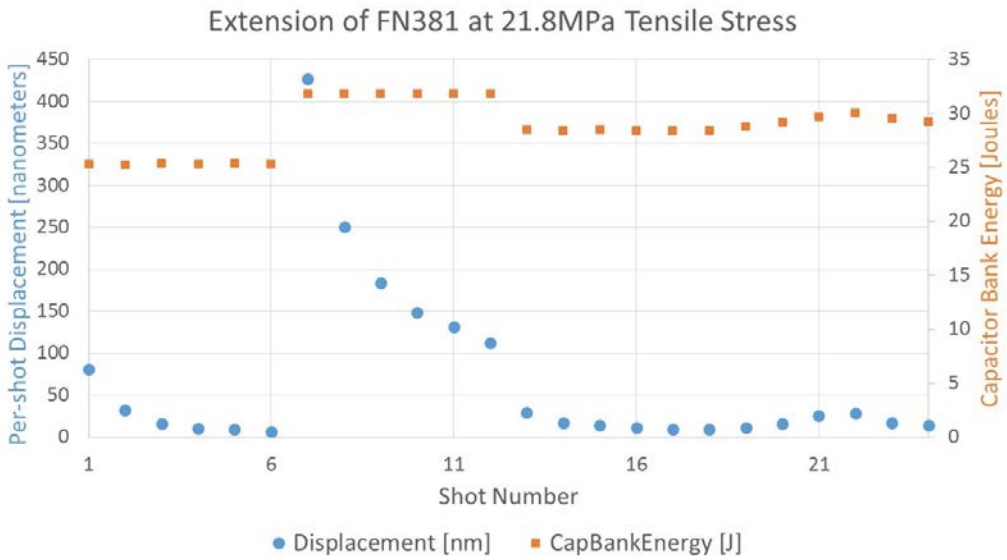

Figure 6. Data[1] gathered with sample under tensile stress. Notice the small increases and decreases in the capacitor bank voltage result in small increases and decreases in actuation displacement.

A zero force experiment was performed by removing the tension springs from the apparatus and discharging the capacitor bank through the sample several times. The capacitor bank was charged to a higher voltage than was used in Figure 6. This zero force data is shown in Figure 7.

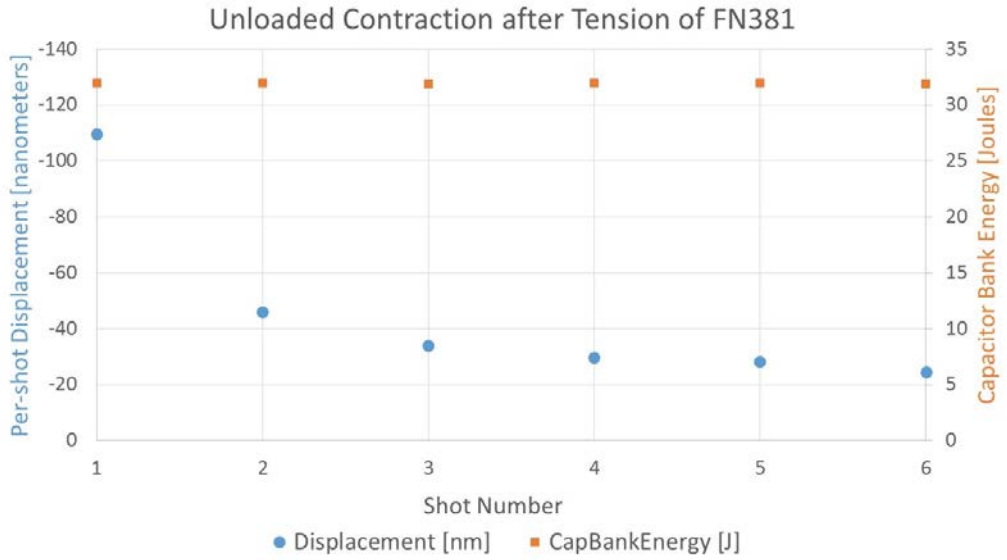

Figure 7. Data[1] gathered with no applied force on the sample. This experiment was performed immediately after the tensile actuations in Figure 6. Notice these actuations are in the opposite direction of the ones in Figure 6.

The same procedure used to gather the FN381 data was used to gather data on the aluminum sample. The data for the aluminum sample is presented in Figures 8, 9, 10, and 11.

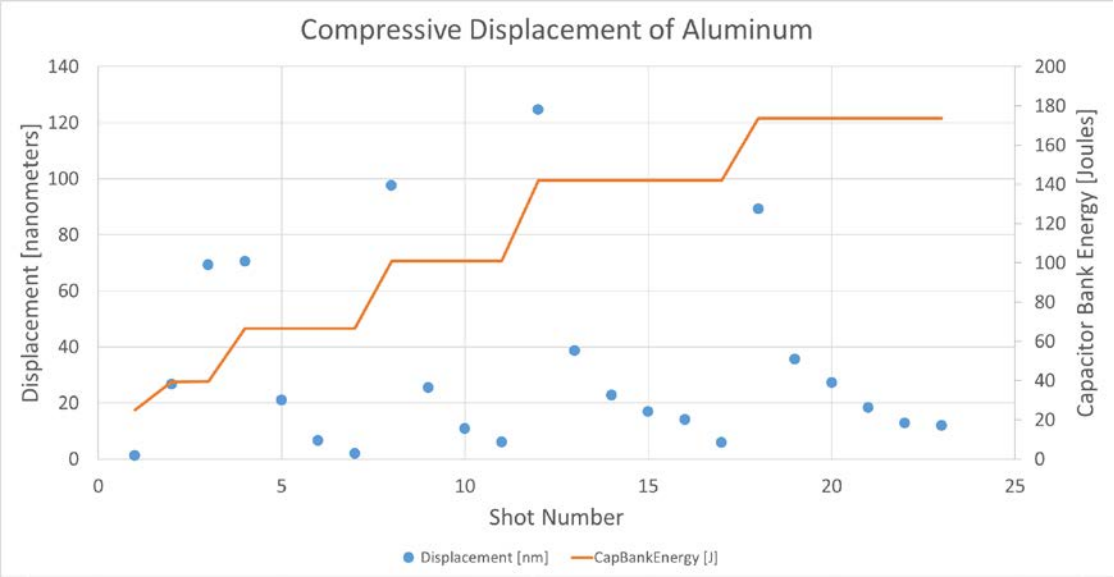

Figure 8. Compressive displacements of the aluminum sample under 59.8 MPa of compressive stress

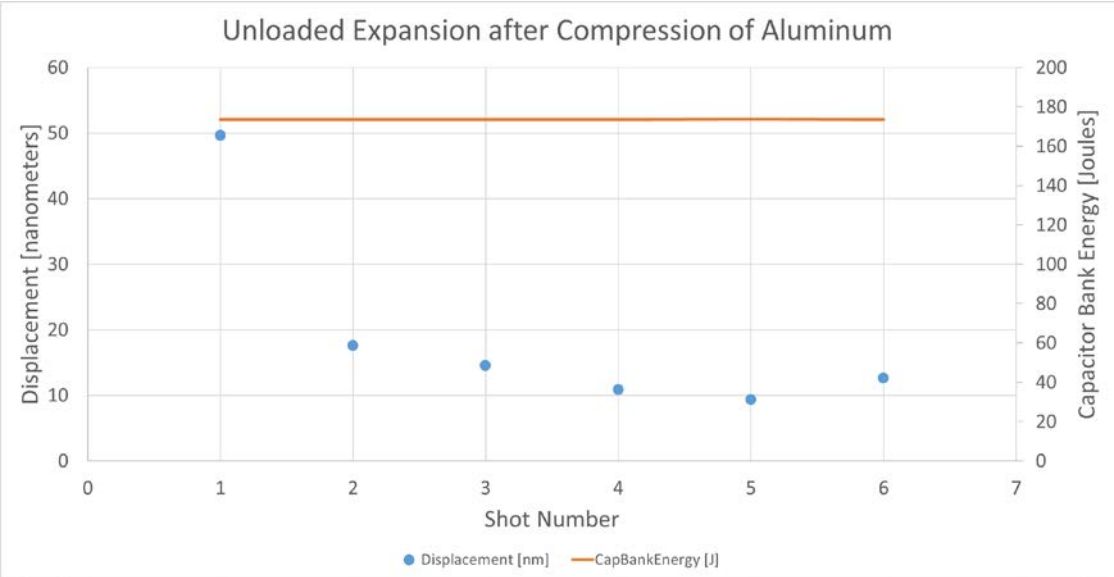

Figure 9. The compressive force was removed from the sample, and the capacitor bank was discharged through the sample

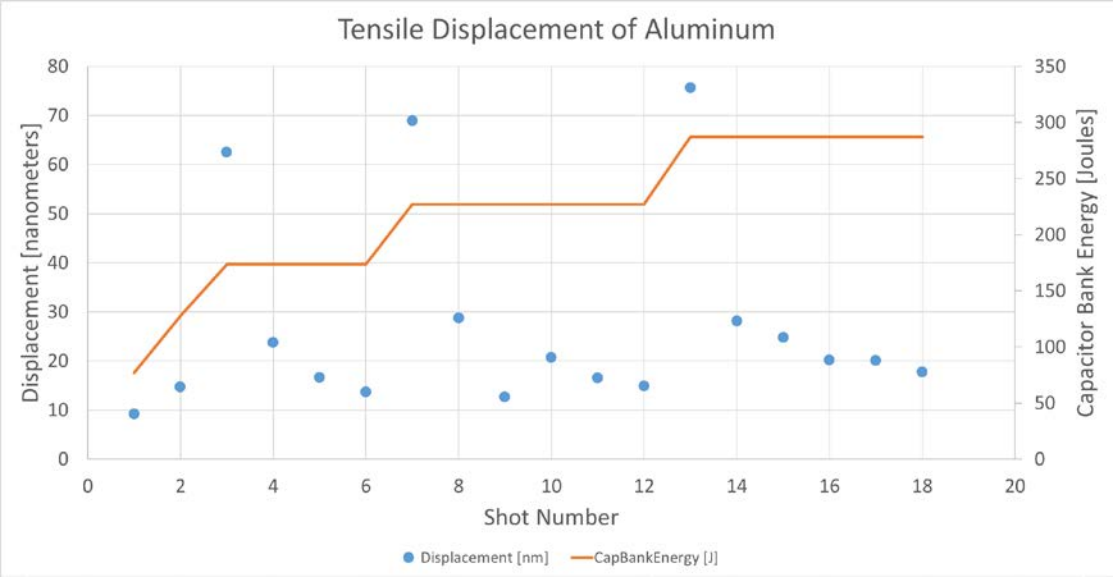

Figure 10. Tensile displacements of the aluminum sample under 37.7 MPa of tensile stress

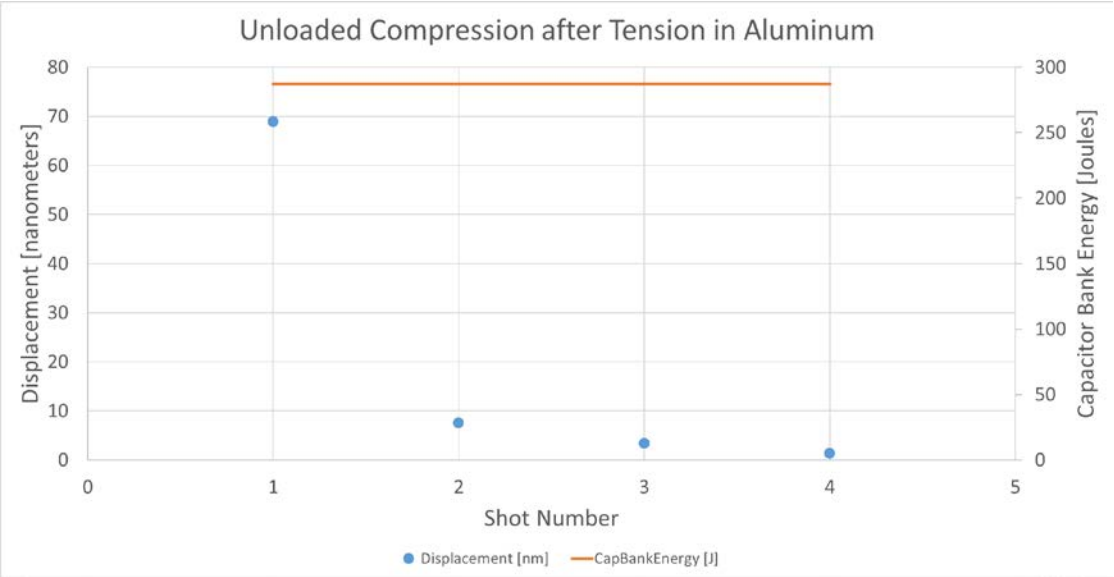

Figure 11. The tensile stress was removed from the aluminum and the capacitor bank was discharged through the sample

Finally, data for the tungsten sample is shown below. The procedure for gathering this data was similar to the procedure for FN381, however tungsten did not exhibit measurable creep at any load. The forces applied to the tungsten sample were determined by the limitations of the apparatus.

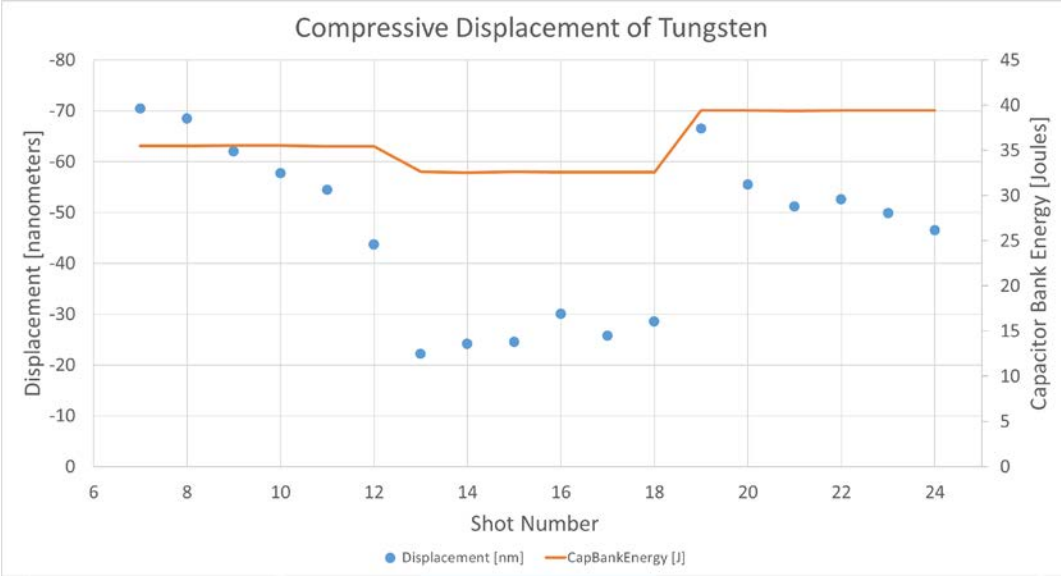

Figure 12. Compressive displacements of the tungsten sample under 66.5 MPa of compressive stress

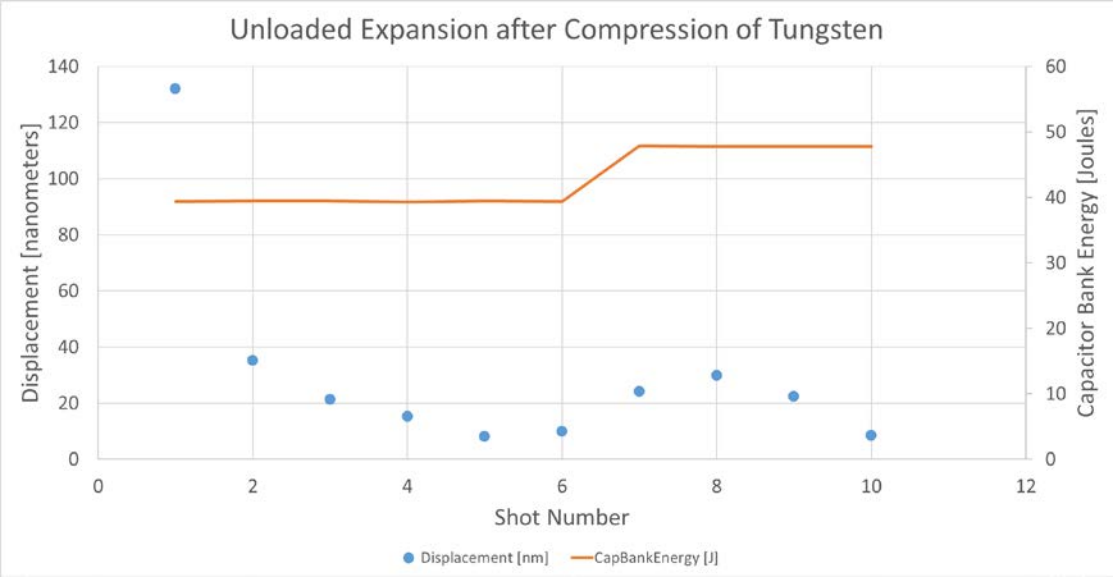

Figure 13. Unloaded displacements of the tungsten sample after the compressive tests

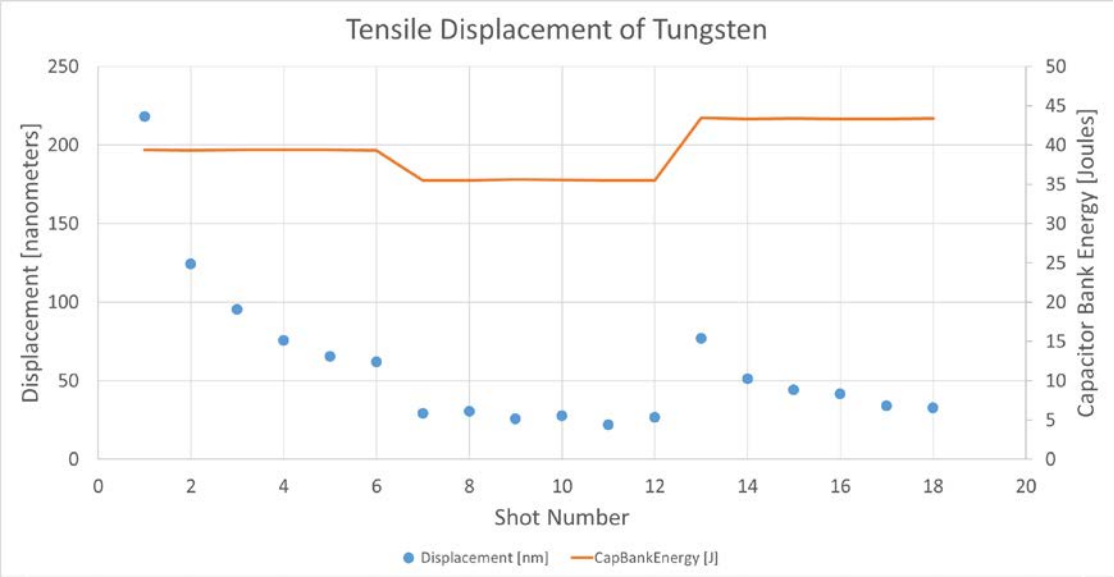

Figure 14. Elongation of the tungsten sample under 50.9MPa of tensile stress

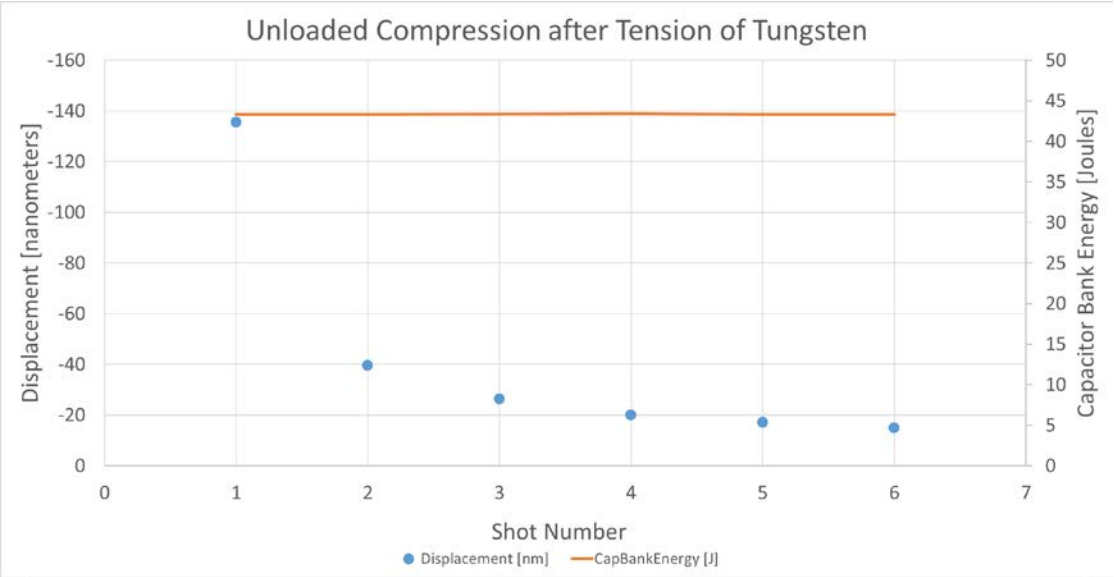

Figure 15. Shortening of the tungsten actuator under no applied force

4. DISCUSSION

4.1 ThermoYield actuator discussion

This data shows several important features of ThermoYield actuators. First, the actuators were demonstrated to achieve metrology-limited actuations as small as 6 nm in both compression and tension. This corresponds to a 0.025 arc-second angle adjustment on a mirror supported by 50 mm spaced actuators. This exceeds the necessary resolution to align mirrors for a 0.5 arc-second mission such as the Lynx X-ray telescope concept. Additionally, the cumulative displacement in each direction is on the order of micrometers, enabling us to start with relatively coarsely made posts and actuate to the desired length.

Second, the data shows a correlation between energy stored in the capacitor bank and actuation displacement. This allows the displacement of actuations to be changed without disturbing the precision assembly. The capacitor bank can be mounted remotely, with energy transferred through long wires. Remote actuation makes it possible to adjust X-

ray telescope optics in a vacuum chamber or X-ray beamline using an electrical feed-through. The data also demonstrates that small changes in the energy stored in the capacitor bank cause small changes in the displacement of subsequent actuations. Large actuations can be used to achieve coarse adjustment, and fine actuations can be used to achieve an exact final length. After the assembly is aligned, the electrical connections can be removed from the actuators, and only the actuator will remain in the assembly.

Finally, ThermoYield actuators were observed to have "memory" of past actuations. The aluminum and tungsten data show that this behavior is present in very different metals. In each trial, the energy and force applied to the actuator were held constant for several actuations; however, each subsequent actuation decreased in displacement. This can be overcome by increasing the energy used to heat the sample. The effect of the sample's memory was also observed in the zero force actuations. The sample moved the opposite direction of the most recent actuations. This may simplify telescope alignment by allowing adjustments without applied force.

5. BOND DEFORMATION LOCALIZATION

Currently, all X-ray telescope assembly methods require bonds to the mirrors, which cause distortion. Two ideas to reduce this distortion (the moat and the bridge) were modeled and simulated in finite element analysis (FEA) software. The moat concept focuses on the addition of circular grooves around the bond area. The moat geometry creates a flexure between the bond area and the rest of the mirror. This model uses a 0.5 mm thick flat silicon mirror with a diameter of 100 mm (Figure 16). The inner radius and outer radius of the frontside moat were 4 mm and 4.1 mm respectively with a 0.35 mm depth. On the backside the inner and outer radii were 3.7 mm and 3.8 mm respectively with a 0.35 mm depth. The distance between the inner wall of the front side moat and the outer wall of the backside moat is 0.1 mm. A 0.001 mm thin film with a diameter of 4 mm was added to the frontside of the mirror. To simulate the bond stress, an integrated film stress of 1 MPa per micron was added in the radial direction across the 4 mm circle surface. This design allows for the stress and deformation due to the epoxy coating to be concentrated in the moat geometry.

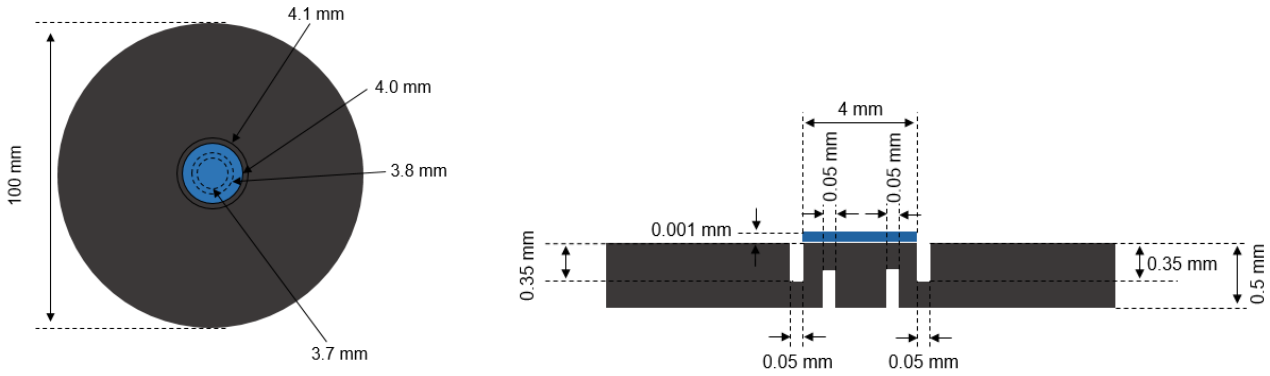

Figure 16. Drawing of the moat concept with dimensions. Not drawn to scale.

To determine the deformation reduction, the simulation was run with and without the moats. The peak-to-valley deformation with and without the moats was 0.347 nm and 1.489 nm respectively, as shown in Figures 17 and 18.

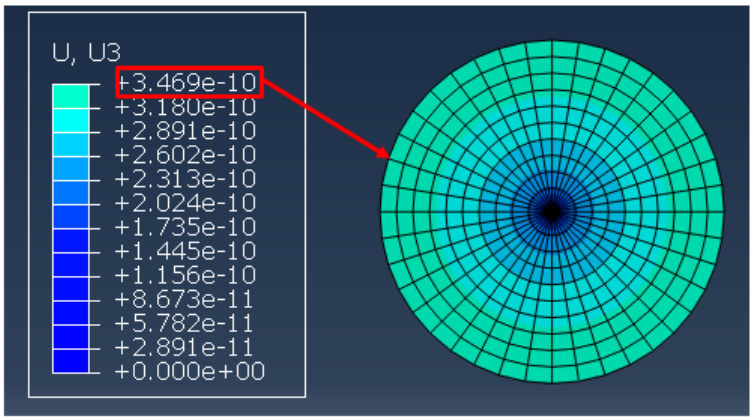

Figure 17. Front and backside moat model with stress coating. Displacements (in meters) caused by the 1 MPa/micron of integrated film stress.

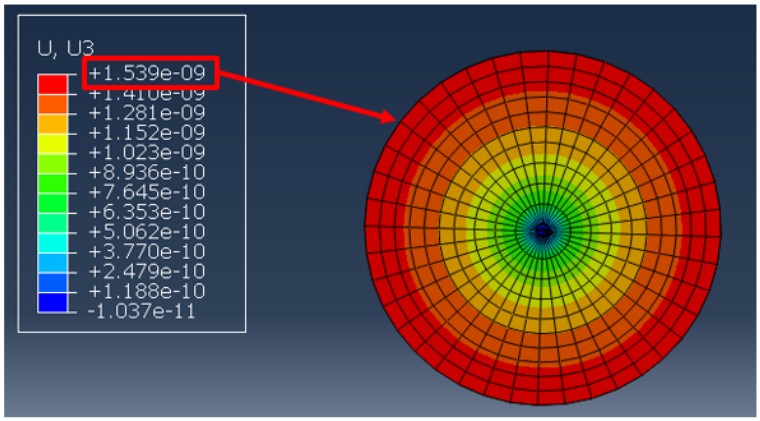

Figure 18. No moat model. Displacements (in meters) caused by the 1 MPa/micron of integrated film stress.

The second concept, which utilized two parallel slits on either side of the bond area, holds the same stress relief principles as the first approach, but with a simpler geometry. This is modeled as a flat silicon square mirror with two slits that run along the sides of the epoxy contact area as shown in Figure 19. The mirror is 100 mm x 100 mm by 0.5 mm thick with two 20 mm x 0.05 mm slits cut all the way through the mirror. There is one slit on each side of a 4 mm by 4 mm square epoxy stress area with a 0.001 mm thickness. A 1 MPa per micron integrated film stress was applied to the 4 mm x 4 mm square tangent to the top surface.

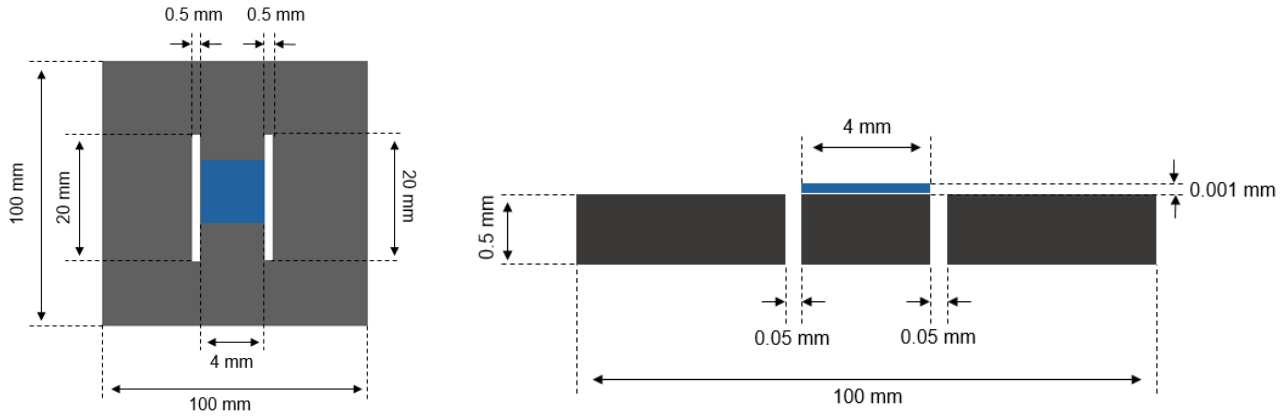

Figure 19. Drawing of the double slit concept with dimensions. Not drawn to scale.

The slit model results were obtained in the same way as the moat model. To determine the deformation reduction, the simulation was run with and without the slits. The peak-to-valley deformation with and without the slits is 1.077 nm and 1.432 nm respectively, as shown in Figures 20 and 21.

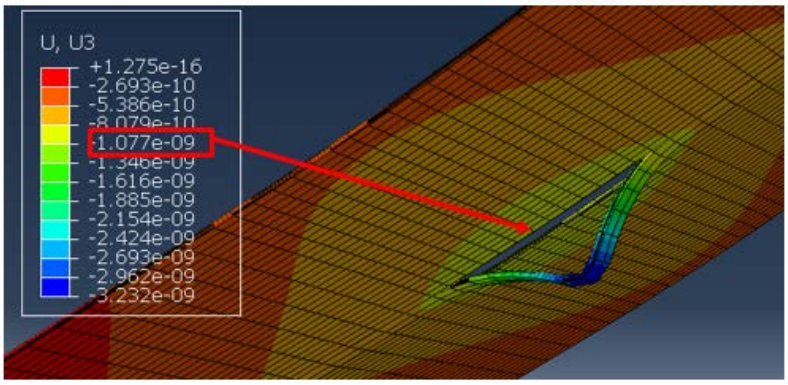

Figure 20. Slit mirror model. Displacements (in meters) caused by the 1 MPa/micron of integrated film stress.

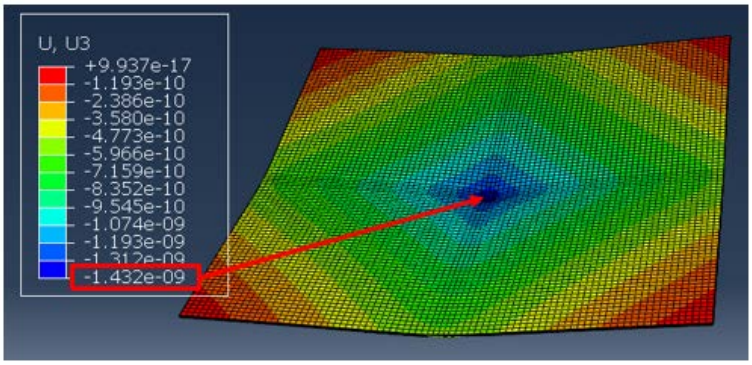

Figure 21. No slit mirror model. Displacements (in meters) caused by the 1 MPa/micron of integrated film stress.

Preliminary results show a peak-to-valley ratio improvement of a factor of 4.3 in the moat model and 1.3 in the slit model. Based on the models produced and the parameters assigned, both approaches showed a reduction in deformation from localization of epoxy coating stress. These results demonstrate that changing the mirror geometry around the bond area can reduce the distortion of the mirror.

These results showed deformation reduction using simplified models. Future work should expand the models to include more realistic X-ray mirrors such as Wolter-I mirrors in a meta-shell with multiple bond points[7].

6. CONCLUSION

In this paper, the concept of ThermoYield actuators is presented as well as its utility for aligning X-ray optics in applications such as the Lynx X-ray telescope concept or the ATHENA X-ray telescope. Results for three different metals are presented via a testing apparatus, and several features of the data are discussed. Length changes as small as 6 nm were demonstrated in both compression and extension. Cumulative length changes on the order of microns were also demonstrated in both directions. A promising idea of using the unloaded "memory" actuations to adjust thin-shell X-ray telescope mirrors without applying external forces was discussed. Additionally, two concepts that involve flexures arrayed around the bond between the mirror and mount were explored via finite element modeling. Both approaches demonstrated significant reduction in peak-to-valley deformation on flat substrates.

ACKNOWLEDGEMENTS

This work was supported by NASA Grant NNX16AD01G. Additional thanks to Will Zhang and others at GSFC for advice and the FN381 metal used in these experiments. Additional thanks to Lester Cohen and others at Harvard-SAO for advice.

REFERENCES

[1] Michael D. DeTienne, Alexander R. Bruccoleri, Brandon Chalifoux, Ralf K. Heilmann, Ross E. Tedesco, Mark L. Schattenburg, "ThermoYield actuators: nano-adjustable set-and-forget optics mounts," Proc. SPIE 10399, Optics for EUV, X-Ray, and Gamma-Ray Astronomy VIII, 103991I (29 August 2017);

[2] Bruccoleri, A. R., Klingensmith, M., Chalifoux, B., Heilmann, R. K., Schattenburg, M. L., "Liquid metal actuators: correctable mounting and assembly of thin-shell x-ray telescope mirrors," Proc. SPIE 9603, Optics for EUV, X-Ray, and Gamma-Ray Astronomy VII, 960312 (4 September 2015);

[3] Koglin, J. E., An, H., Blaedel, K. L., Brejnholt, N.F., Christensen, F. E., Craig, W. W., Decker, T. A., Hailey, C. J., Hale, L. C., Harrison, F. A., Jensen, C. P., Madsen, K. K., Mori, K., Pivovaroff, M. J., Tajiri, G., Zhang, W. W., "NuSTAR hard x-ray optics design and performance," Proc. SPIE 7437, Optics for EUV, X-Ray, and Gamma-Ray Astronomy IV, 74370C (2009);

[4] Brejnholt, N. F., Christensen, F. E., Westergaard, N. J., Hailey, C. J., Koglin, J. E., Craig, W. W., "NuSTAR on-ground calibration: II. Effective area," Proc. SPIE 8443, Space Telescopes and Instrumentation 2012: Ultraviolet to Gamma Ray, 84431Y (2012);

[5] Westergaard, N. J., Madsen, K. K., Brejnholt, N. F., Koglin, J. E., Christensen, F. E., Pivovaroff, M. J., Vogel, J. K., "NuSTAR on-ground calibration: I. Imaging quality," Proc. SPIE 8443, Space Telescopes and Instrumentation 2012: Ultraviolet to Gamma Ray, 84431X (2012);

[6] Gaskin, J. A., Weisskopf, M. C., Vikhlinin, A., Tananbaum, H. D., Bandler, S. R., Bautz, M. W., Burrows, D. N., Falcone, A. D., Harrison, F. A., Heilmann, R. K., Heinz, S., Hopkins, R. C., Kilbourne, C. A., Kouveliotou, C., Kraft, R. P., Kravtsov, A. V., McEntaffer, R. L., Natarajan, P., O'Dell, S. L., Petre, R., Prieskorn, Z. R., Ptak, A. F., Ramsey, B. D., Reid, P. B., Schnell, A. R., Schwartz, D. A., Townsley, L. K., "The X-ray Surveyor Mission: a concept study," Proc. SPIE 9601, UV, X-Ray, and Gamma-Ray Space Instrumentation for Astronomy XIX, 96010J (2015);

[7] McClelland, R. S., Bonafede, J. A., Saha, T. T., Solly, P. M., Zhang, W. W., "Design and analysis of an x-ray mirror assembly using the meta-shell approach," Proc. SPIE 9905, Space Telescopes and Instrumentation 2016: Ultraviolet to Gamma Ray, 99057A (2016);

[8] Chan, K., Zhang, W. W., Schofield, M. J., Numata, A., Mazzarella, J. R., Saha, T. T., Biskach, M. P., McClelland, R. S., Niemeyer, J., Sharpe, M. V., Olsen, L. G., "Alignment and distortion-free integration of lightweight mirrors into meta-shells for high-resolution astronomical x-ray optics," Proc. SPIE 9905, Space Telescopes and Instrumentation 2016: Ultraviolet to Gamma Ray, 99056X (2016);

[9] G. Valsecchi, F. Marioni, G. Bianucci, F. E. Zocchi, D. Gallieni, G. Parodi, M. Ottolini, M. Collon, M. Civitani, G. Pareschi, D. Spiga, M. Bavdaz, E. Wille, "Optical integration of SPO mirror modules in the ATHENA telescope," Proc. SPIE 10399, Optics for EUV, X-Ray, and Gamma-Ray Astronomy VIII, 103990E (29 August 2017);